Novel mediators of anti-tumor immunity: dissecting intratumoral immune responses at the single-cell level

Vries, N.L. de

5

The ILC compartment in mismatch repair-deficient colorectal cancers is dominated by CD127-negative ILC1-like cells

Natasja L. de Vries[1,2], Li Zheng[1], Jessica Roelands[1], Manon van der Ploeg[1], Marieke E. Ijsselsteijn[1], Ruud van der Breggen[1], Juliette Krop[2], Michael Eikmans[2], Dina Ruano[1], Frits Koning[2†], Noel F.C.C. de Miranda[1†]

[1]Department of Pathology, Leiden University Medical Center, Leiden, The Netherlands.
[2]Department of Immunology, Leiden University Medical Center, Leiden, The Netherlands.
[†]Equal responsible authors.

Manuscript in preparation

ABSTRACT

Background

The colorectal cancer (CRC) immune microenvironment is an important determinant of the clinical prognosis of patients. We previously discovered that an unappreciated innate lymphocyte population ($Lin^{-}CD7^{+}CD127^{-}CD103^{+}CD45RO^{+}$) was enriched and displayed hallmarks of cytotoxic activity in mismatch repair (MMR)-deficient CRCs. Little is known about the role of innate lymphoid cells (ILCs) in CRC, and often their analysis has focused on the $CD127^{+}$ compartment. Here, we aimed to characterize the entire $CD7^{+}CD3^{-}CD127^{+/-}$ ILC compartment in MMR-deficient CRCs.

Methods

We performed an unbiased characterization of sorted $CD7^{+}CD3^{-}$ ILCs, independently of CD127 expression, from five patients with MMR-deficient CRC by single-cell RNA-sequencing. In concordance, mass and flow cytometric examination of immunophenotypic markers and transcription factor expression was performed to investigate the full spectrum of ILC subsets and their functional differences.

Results

The majority of ILCs in MMR-deficient CRCs consisted of $CD127^{-}CD103^{+}$ ILC1-like cells, followed by $CD127^{-}CD103^{-}$ NK-like cells, and a minor population of $CD127^{+}CD103^{-}$ conventional ILCs. The ILC1-like cells in CRC tissues specifically expressed CD39, CD45RO, and transcription factor *TBX21* (T-bet). They distinguished from NK-like cells and conventional ILCs by high expression of genes encoding KIRs, co-inhibitory and co-stimulatory molecules, NKG2A, and HLA class II. The ILC1-like cells were the only ILC population displaying hallmarks of proliferation in MMR-deficient CRCs.

Conclusions

Our work provides a comprehensive description of heterogeneity of the ILC population in MMR-deficient CRCs. Validation of our findings in a large CRC dataset confirmed that ILC1-like cells are the dominant ILC subset, which is particularly frequent in MMR-deficient samples. These findings suggest an active involvement of ILCs in the recognition of and cytotoxicity against MMR-deficient cancers, and holds potential for exploiting ILC1-like cells as targets for cancer immunotherapy.

INTRODUCTION

Colorectal cancer (CRC) is distinguished by an extensive and complex tumor microenvironment containing immune cells that impact carcinogenesis and patient prognosis.[1] The advent of immune checkpoint blockade (ICB) targeting the inhibitory PD-1/PD-L1 and/or CTLA-4 axis boosted the anti-tumor potential of cytotoxic T cells, resulting in enhanced immunity via recognition of human leukocyte antigen (HLA) class I-bound (neo)epitopes on cancer cells.[2-4] ICB has provided durable clinical responses in patients diagnosed with mismatch repair (MMR)-deficient CRCs that present with high mutation burden accompanied by an excess of frameshifted neoepitopes.[5-10] However, the large majority of these MMR-deficient CRCs lack expression of HLA class I, due to inactivating mutations in β2-microglobulin (*B2M*), the HLA class I genes themselves, or other components of the antigen processing pathway.[11-14] Hence, these tumors may evade $CD8^+$ T cell-mediated immunity. Interestingly, the majority of HLA class I-negative MMR-deficient CRCs have shown durable responses to ICB,[15] suggesting the involvement of other immune cell subsets than $CD8^+$ T cells.

We previously discovered that an unappreciated ILC1-like population ($Lin^-CD7^+CD127^-CD103^+CD45RO^+$) was enriched in MMR-deficient CRCs and showed high cytotoxic potential.[16] This subset displayed an intraepithelial localization in line with their tissue-resident ($CD103^+CD69^+$) phenotype.[16] ILCs represent a heterogeneous population of innate lymphocytes that reside in mucosal tissues such as the intestine where they have important effector and regulatory functions in infection, inflammation, and tissue remodeling.[17] ILCs lack the expression of rearranged T/B cell receptors and can be activated by cytokines and/or through activating and inhibitory innate immune receptors.[18] They include conventional NK cells as well as ILC1, ILC2, and ILC3 cells that display functional characteristics analogous to the main subsets of helper T cells. ILC1s express the transcription factor *TBX21* (T-bet) and can produce Th1-related cytokines such as IFN-γ, like conventional NK cells. ILC2s are *GATA3*-positive and can secrete Th2-related cytokines (IL-4, IL-5, IL-13). Last, ILC3s express the transcription factor *RORC* (RORγt) and have been described to be involved in IL-17 and IL-22 production.[19] In contrast to conventional NK cells, these ILC subsets display a CD127 (IL-7Rα)-positive phenotype, with the exception of the intraepithelial ILC1 subset,[20] and do not possess cytotoxic activity.[21] Moreover, additional levels of plasticity[22,23] and heterogeneity[24,25] have been described in the ILC classification.

As the intraepithelial ILC1-like ($CD127^-CD103^+CD45RO^+$) population is, in theory, capable of killing cancer cells independently of HLA class I expression, they may be particularly important in mediating anti-tumor immune responses in MMR-deficient CRCs, also in the therapeutic setting with ICB therapy. Here, we performed single cell-level analysis on the entire $CD7^+CD3^-CD127^{+/-}$ ILC population derived from MMR-deficient CRCs, including single-cell RNA-sequencing, flow cytometry, and mass cytometry. We find that the ILC compartment in MMR-deficient CRCs is dominated by $CD127^-CD103^+$ ILC1-like cells that exhibit a transcriptional profile related to cancer immunity.

RESULTS

Majority of ILCs in MMR-deficient colorectal cancers are CD127$^-$CD103$^+$ ILC1-like cells
Characterization of the CD7$^+$CD3$^-$CD127$^{+/-}$ ILC population in MMR-deficient CRCs by mass cytometric analysis (**Figure S1**, **Table S1**, **Table S2**) showed that the majority of the ILCs that infiltrate these tumors lack expression of conventional ILC marker CD127 (IL-7Rα) (**Figure 1A**). The majority of the CD7$^+$CD3$^-$ cells consisted of CD127$^-$CD103$^+$ ILC1-like cells, followed by a CD127$^-$CD103$^-$CD56$^{dim/bright}$ NK-like population, and a minor population of CD127$^+$ conventional ILCs (**Figure 1A**). The majority of CD127$^-$CD103$^+$ ILC1-like cells also expressed ectonucleotidase CD39, CD56, and CD45RO, whereas a minor population of CD127$^-$CD103$^+$CD45RA^{dim} cells was observed (**Figure 1A,B**). Nevertheless, CD45RA expression was mainly detected in the CD127$^-$CD103$^-$CD56$^{dim/bright}$ NK-like population (**Figure 1A,B**). Last, the CD127$^+$ conventional ILCs showed a CD45RA$^{+/-}$ phenotype (**Figure 1A,B**). Across four patients with MMR-deficient CRC, the CD127$^-$CD103$^+$CD45RO$^+$ ILC1-like population was the most prevalent constituting up to 75% (average 55%) of the total CD7$^+$CD3$^-$CD127$^{+/-}$ ILC population (**Figure 1C**). In addition to the aforementioned immune cell markers, the CD103$^+$ ILC1-like cells also expressed high levels of CD38 and CD69 (**Figure 1D**).

The CD127$^+$ conventional ILC population showed co-expression of the transcription factor *GATA3*, but not of *TBX21* (T-bet), *EOMES* or *RORC* (RORγt), indicating an ILC2 phenotype (**Figure 1E**). The CD127$^-$CD103$^+$CD45RO$^+$ population expressed *TBX21*, in line with their ILC1-like phenotype (**Figure 1E**). Both CD127$^-$CD103$^+$CD45RA^{dim} and CD127$^-$CD103$^-$CD45RA$^+$ populations showed the co-expression of *TBX21* and *EOMES*, indicative of a conventional NK cell phenotype (**Figure 1E**). Cytotoxic molecules granzyme B and perforin were highly expressed by all ILC populations, with the exception of the CD127$^+$ ILC2s (**Figure 1F**). NKp44, a marker used to characterize intraepithelial ILC1s,[20] was expressed at variable levels by the ILC1-like cells (**Figure S2**). We next investigated the presence of receptors recognizing HLA class I molecules. CD94 and NKG2A, able to bind to the non-classical HLA-E protein,[26] were highly expressed by the ILC1-like cells, and to a lower extent by the NK cell-like and ILC2 populations (**Figure S2**). Killer-cell immunoglobulin-like receptors (KIRs), recognizing different HLA class I molecules, were expressed by the ILC1-like and NK cell-like populations at variable levels, and to a lower extent by the ILC2 cells (**Figure S2**).

Figure 1. Majority of ILCs in MMR-deficient colorectal cancers are CD127$^-$CD103$^+$ ILC1-like cells.
A. t-SNE embedding showing 6.0x10^4 CD7$^+$CD3$^-$ innate lymphoid cells (ILCs) isolated from MMR-deficient CRCs (N=4) analyzed by mass cytometry. Colors represent relative expression of indicated immune cell markers. **B**. t-SNE embedding of (**A**) colored by ILC subsets. **C**. Circular plot showing the relative frequency of ILC subsets as average percentage of total CD7$^+$CD3$^-$ ILCs from MMR-deficient CRCs (N=4). **D.** Expression (ArcSinh5-transformed) of surface markers of CD127$^-$CD103$^+$CD45RO$^+$ ILC1-like (orange), CD127$^-$CD103$^+$CD45RA^{dim} ILC1-like (pink), CD127$^-$CD103$^-$CD45RA$^+$ NK-like (purple), and CD127$^+$CD103$^-$CD45RA$^{+/-}$ ILC2 (green) cells from MMR-deficient CRCs (N=4). **E.** Expression (ArcSinh5-transformed) of intracellular transcription factors and cytotoxicity markers of CD127$^-$CD103$^+$CD45RO$^+$ ILC1-like (orange), CD127$^-$CD103$^+$CD45RA^{dim} ILC1-like (pink), CD127$^-$CD103$^-$CD45RA$^+$ NK-like (purple), and CD127$^+$CD103$^-$CD45RA$^{+/-}$ ILC2 (green) cells from MMR-deficient CRCs (N=4).

We explored the full composition of the ILC compartment in MMR-deficient CRCs, independently of CD127 expression, by performing single-cell RNA-sequencing (scRNA-seq) on *ex vivo* isolated CD7^{+}CD3^{-}CD127$^{+/-}$ cells (**Figure S3, Table S1**). As the CD45 isoforms CD45RA and CD45RO cannot be detected at the RNA level, we included two CITE-sequencing antibodies against these markers (**Figure S3**). Transcriptomes were obtained from a total of 4270 ILCs and used for further analysis (**Figure S3**). A patient-specific analysis approach was performed to avoid loss of biologically-relevant populations upon integrating the scRNA-seq data of the different patients. Three to six distinct ILC clusters were identified per patient and visualized by t-SNE (**Figure 2A**). In each patient, we observed the presence of an *IL7R*$^{+}$*ITGAE*$^{-}$ (CD127^{+}CD103^{-}) conventional ILC cluster (except for CRC159), *IL7R*$^{-}$*ITGAE*$^{+}$ (CD127^{-}CD103^{+}) ILC1-like clusters, and *IL7R*$^{-}$*ITGAE*$^{-}$ (CD127^{-}CD103^{-}) NK-like clusters (**Figure 2A,B**). The ILC1-like clusters showed co-expression of CD45RO protein (antibody-derived tag, ADT), whereas CD45RA (ADT) protein expression was mainly found on the conventional ILC and/or NK-like clusters (**Figure 2A,B**). In line with the mass and flow cytometric data, the majority of the cells consisted of CD103^{+} ILC1-like cells, followed by NK-like cells, and a minor population of conventional ILCs (**Figure 2C**). Also in line with the protein data, the CD127^{+} conventional ILCs expressed *GATA3*, confirming their ILC2 phenotype (**Figure S4**).

CD127^{-}CD103^{+} ILC1-like cells exhibit a transcriptional profile related to cancer immunity

We next examined what functionally distinguished the different ILC clusters identified using differential expression analysis for each patient. Across patients, clusters with similar significantly differential expressed genes could be detected (**Figure 3A**, **Figure S5**). Differentially expressed genes for the CD103^{+} ILC1-like clusters across patients included genes encoding co-inhibitory and co-stimulatory molecules, KIRs, cytotoxicity markers, and HLA class II molecules (**Figure 3A**, **Figure S5**). As compared to the other populations, the CD103^{+} ILC1-like cells showed high expression of *ENTPD1* (CD39), activating receptor *KLRB1* (CD161), inhibitory receptor *KLRC1* (NKG2A), and activating receptor *NCR2* (NKp44) (**Figure 3B**). Genes encoding co-inhibitory (TIGIT, TIM3, LAG3) and co-stimulatory molecules (4-1BB) were also expressed mainly by the CD103^{+} ILC1-like cells (**Figure 3B**). CD103^{+} ILC1-like cells highly expressed *KIRs* as compared to the other populations (**Figure 3B**). Across all patients, the most commonly expressed KIR was *KIR2DL4*, which can bind to HLA-G molecules.[27] Of all ILC populations, the CD103^{+} ILC1-like cells were the only ones displaying hallmarks of proliferation (*MKI67*$^{+}$) in MMR-deficient CRCs (**Figure 3B**).These *MKI67*+ proliferating ILC1-like clusters commonly co-expressed genes encoding co-inhibitory and co-stimulatory molecules, KIRs, cytotoxicity markers, and HLA class II molecules (**Figure 3B**, **Figure S5**). The most frequently expressed interleukin receptors in the CD103^{+} ILC1-like population were *IL2RB*, and to a lower extent *IL2RG*, *IL4R*, *IL10RA*, and *IL21R* (**Figure S6**). Abundant expressed interleukin transcripts were *IL32*, and to a lower extent *IL16* (**Figure S6**).

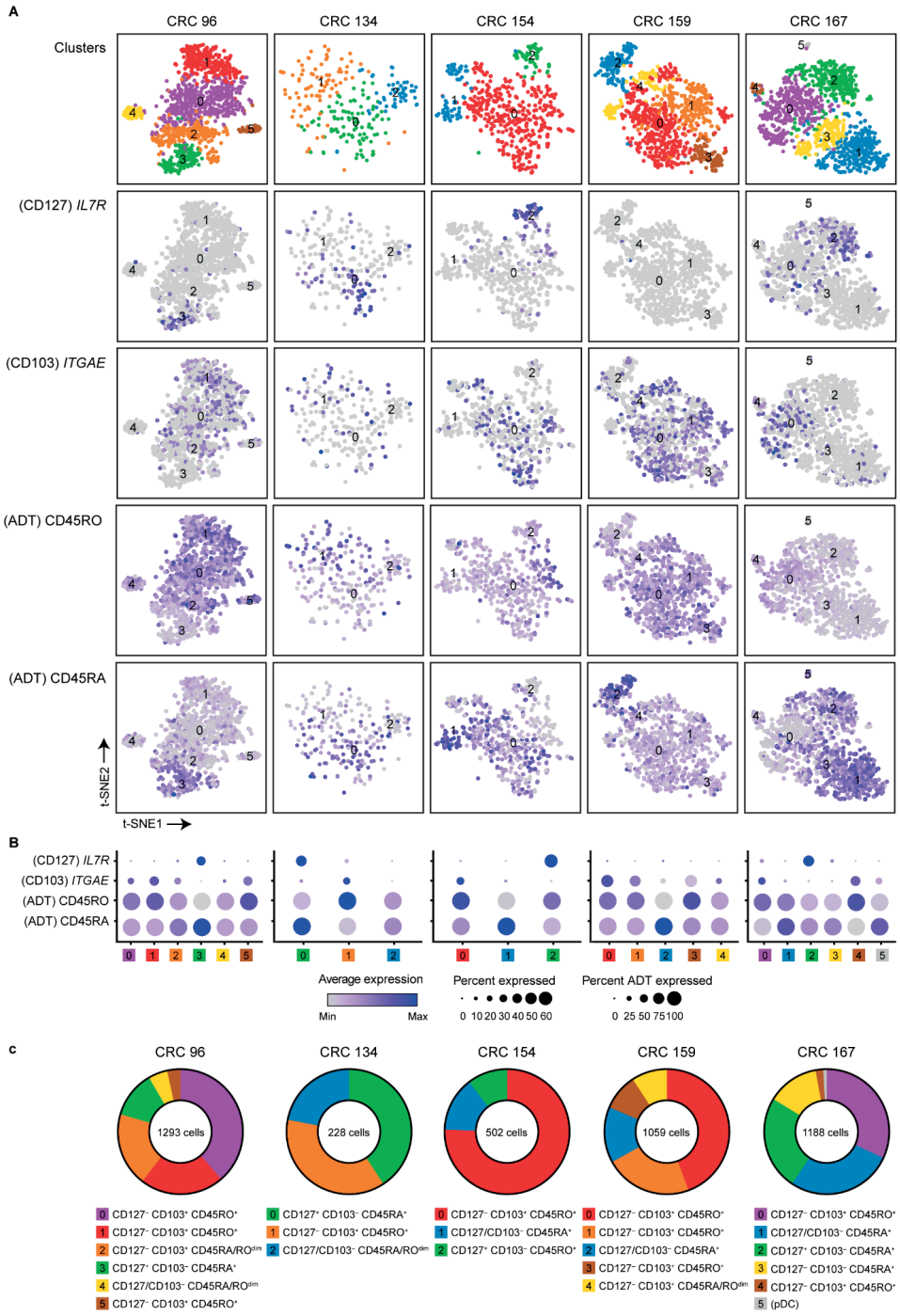

Figure 2. Unbiased, single-cell characterization of ILC populations in MMR-deficient colorectal cancers.
A. t-SNE embedding showing the clustering of CD7^{+}CD3^{-} ILCs isolated from MMR-deficient CRCs (N=5) analyzed by single-cell RNA-sequencing per patient. Colors represent functionally distinct ILC clusters (top row) and relative expression of indicated genes and proteins (remainder). Each dot represents a single cell. ADT; antibody-derived tag. **B**.

Dot plots showing the relative expression of indicated markers in the clusters identified in (**A**). Color intensity indicates average expression and size of the dot indicates the percentage of cells expressing the gene or protein. ADT; antibody-derived tag. **C**. Circular plots showing the frequencies of the distinct ILC clusters identified in (**A**) as a percentage of total $CD7^{+}CD3^{-}$ ILCs per patient.

Differentially expressed genes for the NK-like clusters across patients included genes encoding cytotoxicity markers and chemokines (**Figure 3A**, **Figure S5**). NK-like cells showed high expression of *FCG3RA* (encoding CD16), *NKG7* (NK cell granule protein), *KLRD1* (CD94), and activating receptors *KLRF1* (NKp80), *NCR1* (NKp46) and *NCR3* (NKp30) (**Figure 3B**). Both ILC1-like and NK-like clusters highly expressed cytotoxic molecules *GNLY*, *GZMB*, and *PRF1* as well as proinflammatory cytokine *IFNG* (**Figure 3B**). In opposition to $CD103^{+}$ ILC1-like cells, the NK-like cells generally showed lower expression of genes encoding co-inhibitory and co-stimulatory receptors and KIRs, and lacked expression of proliferation marker *MKI67* (**Figure 3B**). The NK-like clusters further distinguished from the other populations by high expression of chemokines CCL3 and/or CCL4 (**Figure 3B**). Interleukin receptor *IL2B* was expressed by the NK-like clusters, but to a lower extent than the $CD103^{+}$ ILC1-like cells (**Figure S6**). Last, differentially expressed genes for the ILC2 clusters across patients included *FOS* (transcriptional regulation), *XCL1* (lymphotactin), *KIT* (c-kit), *LTB* (regulation of inflammation), *SELL* (CD62L), and *NFKBIA* (IκBα) (**Figure 3A**, **Figure S5**). The ILC2 cells generally lacked expression of co-inhibitory and co-stimulatory molecules, KIRs, and cytotoxic molecules, with some exceptions (**Figure 3B**). Further, generally no expression of genes encoding chemokines CCL3, CCL4 or CCL5, HLA class II molecules, and proliferation marker Ki-67 were found in the ILC2s (**Figure 3B**). Importantly, the majority of the entire ILC population in MMR-deficient CRCs lacked expression of co-inhibitory receptors and immune checkpoint molecules *PDCD1* (PD-1) and *CTLA4*, both at the RNA and protein level (**Figure 3B**, **Figure S7**). Taken together, as compared to NK-like cells, the ILC1-like cells specifically express genes encoding CD103, CD39, CD161 and NKG2A, more frequently express genes encoding co-inhibitory and co-stimulatory molecules, KIRs and HLA class II, and display hallmarks of proliferation in MMR-deficient CRCs.

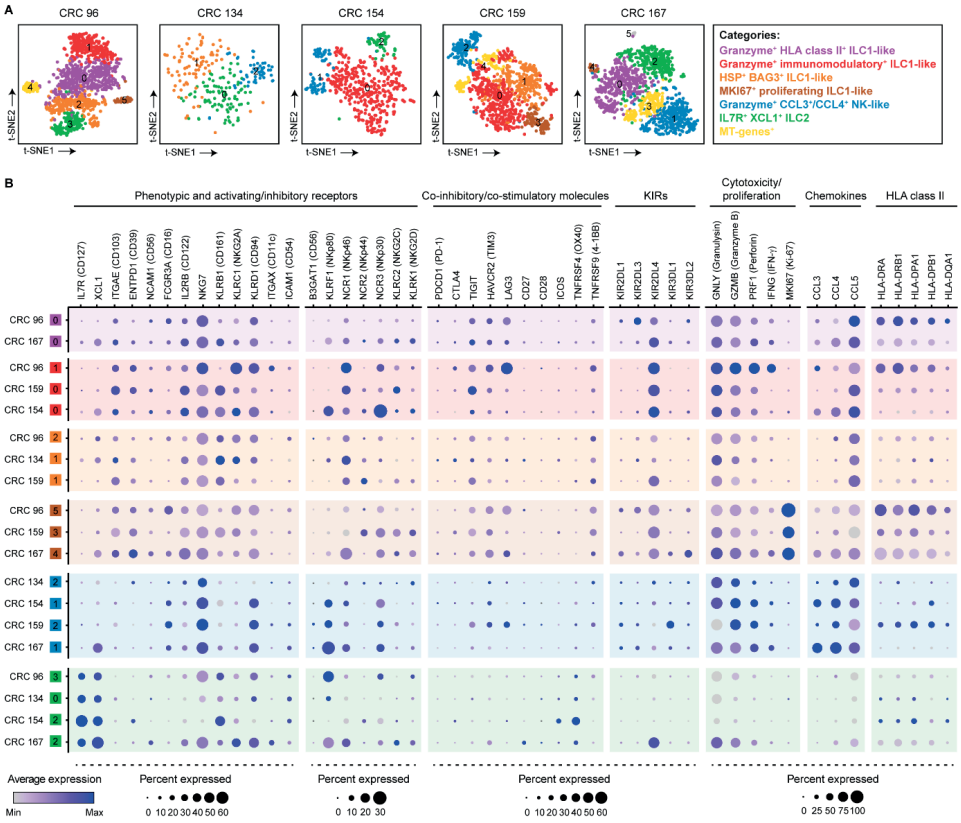

Figure 3. CD127⁻CD103⁺ ILC1-like cells exhibit a transcriptional profile related to cancer immunity.
A. t-SNE embedding showing the clustering of CD7⁺CD3⁻ ILCs from MMR-deficient CRC 96 (N=1293), CRC 134 (N=288), CRC 154 (N=502), CRC 159 (N=1059), and CRC 167 (N=1188) analyzed by single-cell RNA-sequencing. The top ten differentially expressed genes of the distinct ILC clusters are shown in **Figure S5**. Colors indicate functionally distinct categories of ILC subsets. Each dot represents a single cell. **B**. Dot plots showing the relative expression of indicated genes in the clusters identified in (**A**). Color intensity indicates average expression and size of the dot indicates the percentage of cells expressing the gene. Background colors indicate functionally distinct categories of ILC subsets as in (**A**).

Last, we validated our findings in a publicly available scRNA-seq cohort[28] consisting of MMR-deficient CRCs, MMR-proficient CRCs, and adjacent healthy tissues. This dataset confirmed that the majority of the ILC population consisted of ILC1-like cells that were particularly abundant in MMR-deficient CRCs, in line with our observations (**Figure 4A-C**).

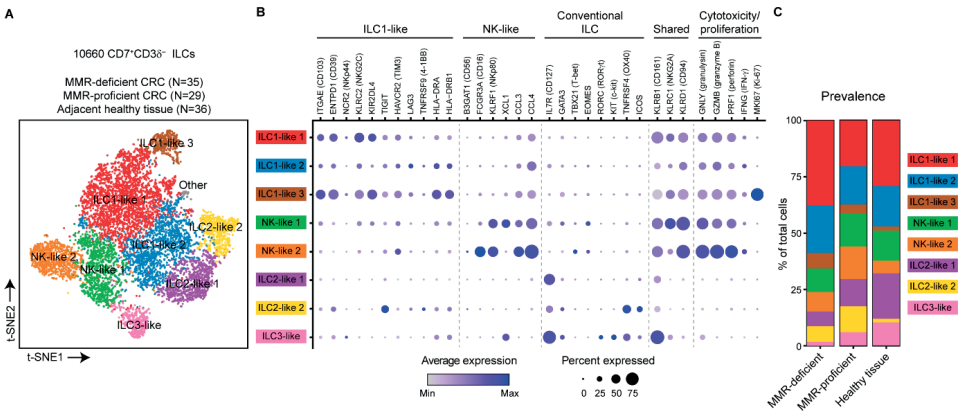

Figure 4. Validation of the abundance and transcriptional profile of CD127^{-}CD103^{+} ILC1-like cells in an independent CRC cohort.
A. t-SNE embedding showing the clustering of CD7^{+}CD3δ^{-} ILCs (N=10660) from MMR-deficient CRCs (N=35), MMR-proficient CRCs (N=29), and adjacent healthy tissues (N=36) obtained from the single-cell RNA-sequencing dataset of Pelka *et al.*[28]. The top ten differentially expressed genes of the distinct ILC clusters are shown in **Figure S9**. Each dot represents a single cell. **B**. Dot plots showing the relative expression of indicated genes in the clusters identified in (**A**). Color intensity indicates average expression and size of the dot indicates the percentage of cells expressing the gene. **C**. Prevalence of the clusters identified in (**A**) among MMR-deficient CRCs, MMR-proficient CRCs, and adjacent healthy tissues shown as percentage of total cells.

5

DISCUSSION

In this work, we provide an unbiased, single-cell characterization of CD7^{+}CD3^{-}CD127$^{+/-}$ ILCs from MMR-deficient CRCs. We defined biological heterogeneity within the ILC population through scRNA-seq, flow cytometry, and mass cytometry on thousands of individual ILCs, independently of CD127 expression. Unsupervised clustering of ILCs distinguished ILC1-like (CD127^{-}CD103^{+}), NK-like (CD127^{-}CD103^{-}), and conventional ILC (CD127^{+}CD103^{-}) subsets across different patients, and we defined the similarities and differences between these ILC subsets. Specifically, we showed that i) the major ILC population in MMR-deficient CRCs consisted of CD127^{-}CD103^{+} ILC1-like cells, ii) these ILC1-like cells specifically expressed CD39, CD45RO, and transcription factor T-bet, iii) high expression of genes encoding KIRs, co-inhibitory and co-stimulatory molecules, NKG2A, and HLA class II distinguished the ILC1-like cells from NK-like cells and conventional ILCs, and iv) the ILC1-like cells are actively proliferating in MMR-deficient CRCs.

The role of ILCs in colorectal cancer immunity and immunotherapy remains largely unclear. Recent single-cell transcriptome characterizations specifically focused on the Lin^{-}CD127^{+} compartment in healthy and malignant colorectal tissue.[29,30] Here, we aimed to characterize the entire CD7^{+}CD3^{-} ILC compartment, independently of CD127 expression, in MMR-deficient CRCs. Our results revealed that the CD127^{+} conventional ILC population is a relative small subset of the total ILC population in CRC tissues, whereas CD127^{-}CD103^{+}

ILC1-like cells and CD127$^-$CD103$^-$ NK-like cells are present in larger frequencies. Such intraepithelial ILC1-like cells have been described to be found in solid tumors, resembling the ones described in the mass cytometry study of lung and colorectal tumors of Simoni *et al.*[31] In line with their study, NKp44, a marker used to characterize intraepithelial ILC1 cells,[20] was not or infrequently observed on the ILC1-like cells in CRC tissues (**Figure S2**). We found that the CD103$^+$ ILC1-like cells could express *IL2RB* and, to a lower extent, *IL2RG*, known to transduce signals by IL-15 in addition to IL-2. IL-15 is a common γ-chain cytokine that can be expressed by epithelial cells and is critical for the maintenance of intestinal intraepithelial lymphocytes,[32] in line with their intraepithelial localization. In contrast to the study of Simoni *et al.* that reported a low expression of cytotoxic granule components,[31] we did observe that the CD103$^+$ ILC1-like cells exhibited a high expression of cytotoxic molecules and IFN-γ. Cytotoxicity and tumor-specific expansion of CD127$^-$CD103$^+$ ILC1-like cells have been shown in murine cancer models, which contrasted the lack of cytotoxicity in the distinct population of CD127$^+$CD103$^-$ conventional ILC1.[33] We found consistent co-expression of CD103, CD39 and CD45RO on the ILC1-like population, implying that these markers can be used to identify the cells. In our study, the CD103$^+$ ILC1-like populations appeared to be transcriptionally distinct but related to conventional NK cells, as has been described before,[31,34] with regard to expression of activating and/or inhibitory innate immune receptors and cytotoxicity markers. In addition, the CD103$^+$ ILC1-like cells showed characteristics of tissue-resident cytotoxic T cells in terms of expression of tissue-residency markers, co-inhibitory and co-stimulatory molecules, cytotoxicity markers, and the expression of transcripts encoding variable regions of the TCR. We found gene expression of CD3ε as well as TRCδ, TRCα, and TCRβ by the ILCs (**Figure S8**), in line with what others have reported.[35-37] TCR rearrangement and clonality of the ILCs will be subject of future studies.

Although previous studies in murine models reported on PD-1 and/or CTLA-4 expression on NK cells and ILC2s in other cancer types and their subsequent involvement in mediating responses to PD-1/PD-L1 blockade,[38-40] the majority of CD7$^+$CD3$^-$ ILCs in MMR-deficient CRCs lacked expression of immune checkpoint molecules PD-1 and CTLA-4. This highlights the need to further investigate the contribution of ILCs in response to PD-1/PD-L1 blockade immunotherapy in human cancer and the involvement of other immune cells such as CD4$^+$ T cells. We found that the ILC1-like cells express high levels of HLA class I-binding receptors KIRs, CD94, and NKG2A, which may sense the lack of HLA class I expression on the cancer cells. KIR2DL4 was the most frequently expressed KIR across all five patients, and has been shown to function as an activating receptor involved in cytokine and chemokine secretion of which the sole ligand known is HLA-G[27]. CD94/NK2G2A is an inhibitory receptor able to bind to the non-classical HLA-E protein,[26,41] suggesting that blocking NKG2A may result in an increased effector function of the CD103$^+$ ILC1-like cells, which will be tested in future functional studies. Last, the expression of HLA class II by CD103$^+$ ILC1-like cells may suggest that these cells have antigen-presenting properties, an interesting direction for further exploration.

Our study is limited with respect to the unraveling of heterogeneity within the CD127$^+$ conventional ILC population, as these cells were present at low frequencies (average 9.7%

of the total CD7^{+}CD3^{-} population; **Figure 1C**). The CD127^{+} ILCs were positive for GATA3, indicating an ILC2 phenotype, in line with other studies on ILC2s in CRC.[29] No RORγt^{+} ILC3s could be detected in our cohort of MMR-deficient CRCs, while we detected an ILC3 cluster in the dataset of Pelka *et al.*[28] that was mainly derived from adjacent healthy tissues. Previous studies reported on remarkably decreased ILC3 populations in colorectal tumor tissues,[29,42-44] albeit being present at high frequencies in healthy colon tissues.[30,31,42] Studies have shown plasticity of ILC3s into ILC1-like cells driven by the presence of cytokines such as IL-12, IL-23, TGF-β in the microenvironment of CRCs.[22,45] In addition, ILC1-like phenotypes could emerge from NK cell differentiation driven by TGF-β signaling in murine cancer models.[46] It remains to be determined what the precursor of the CD103^{+} ILC1-like cells is in colorectal tumors and whether they can further differentiate into other ILC populations depending on environmental signals. In general, the conventional CD127^{+} ILCs in our study did not show expression of cytotoxic molecules both at the transcriptome and protein level, in line with what others found.[17] We will examine the localization and interacting cells of the different ILC populations with imaging mass cytometry. The expression of intracellular CD3ε and TCRs complicates the detection of these cells in tissues. We found that the ILCs lacked expression of (intracellular) CD3δ, a marker we are currently employing to pinpoint the cells by imaging mass cytometry in colorectal tumors with and without HLA class I expression, accompanied by functional studies.

In conclusion, this study provides a comprehensive description of heterogeneity of the ILC population in MMR-deficient CRCs. Our results point toward an active involvement of ILCs in the recognition of and cytotoxicity against MMR-deficient cancers. Our findings may facilitate the exploitation of ILC1-like cells as targets for cancer immunotherapy, and thereby broadening the potential of tumor-resident immune cell populations.

METHODS

Patient samples

Primary CRC tissues (N=10) were from a total of nine patients with CRC undergoing surgical resection of their tumor at the Leiden University Medical Center (LUMC, the Netherlands) (**Table S1**). All patients were treatment-naïve, and did not have a previous history of inflammatory bowel disease. One patient was diagnosed with multiple primary colorectal tumors at different locations, two of which were included in this study. All patients included in this study provided written informed consent. The study was approved by the Medical Ethical Committee of the Leiden University Medical Center (protocol P15.282). All specimens were anonymized and handled according to the ethical guidelines described in the Code for Proper Secondary Use of Human Tissue in the Netherlands of the Dutch Federation of Medical Scientific Societies.

Processing of colorectal cancer tissues

Details on the processing of primary CRC tissues have been described previously.[16] Briefly, macroscopic sectioning from the lumen to the most invasive area of the tumor was performed. Tissue specimens were collected in IMDM+Glutamax medium (Gibco) with 20% fetal calf serum (FCS) (Sigma-Aldrich), 1% pen/strep (Gibco) and fungizone (Gibco), and 0.1% ciprofloxacin (provided by apothecary LUMC) and gentamicin (Invitrogen). Tissues were minced into small fragments in a petri dish, followed by enzymatical digestion with 1 mg/mL collagenase D (Roche Diagnostics) and 50 µg/mL DNase I (Roche Diagnostics) in 5 mL IMDM+Glutamax medium for 30 min at 37°C in gentleMACS C tubes (Miltenyi Biotec). Cell suspensions were dissociated mechanically during and after incubation using the gentleMACS Dissociator (Miltenyi Biotec). Thereafter, cell suspensions were filtered through a 70-µm cell strainer (Corning) and washed in IMDM+Glutamax medium with 20% FCS, 1% pen/strep, and 0.1% fungizone. Cell count and viability were determined with the Muse Count & Viability Kit (Merck) on the Muse Cell Analyzer (Merck), and cells were cryopreserved in liquid nitrogen based on the number of viable cells in IMDM+Glutamax medium complemented 1:1 with 80% FCS and 20% dimethyl sulfoxide (DMSO) (Merck).

Immunohistochemical detection of MMR, β2m, and HLA class I

MMR status of CRC tissues was examined by immunohistochemical staining of PMS2 (anti-PMS2 antibodies; clone EP51, DAKO) and MSH6 (anti-MSH6 antibodies; clone EPR3945, Abcam) proteins.[47] Tumor samples showing the lack of expression of at least one of the MMR-proteins in the presence of an internal positive control were defined as MMR-deficient. Further, β2m expression on CRC tissues was determined by immunohistochemical staining of β2m (anti-β2m antibodies; clone EP2978Y, Abcam). Last, immunohistochemical staining of HLA class I expression on CRC tissues was performed with HCA2 and HC10 monoclonal antibodies (Nordic-MUbio), and classified as HLA class I positive, weak, or loss as described previously.[14]

Mass cytometry staining and data analysis

Mass cytometric analysis was performed on four MMR-deficient CRC tissues with an antibody panel of 44 immune cell markers covering immune lineage markers, differentiation/activation markers, co-inhibitory and co-stimulatory molecules, adhesion molecules, transcription factors, and cytotoxicity markers (**Table S2**). Briefly, single-cell suspensions were thawed and Percoll (GE Healthcare) density-gradient centrifugation was performed to isolate immune cells. Cells were washed in Maxpar Cell Staining Buffer complemented with EDTA (CSB, Fluidigm) and counted. Up to 3 million cells of each sample were incubated with 1 mL CSB containing 1 µM Cell-ID intercalator-103Rh (Fluidigm) for 15 min at room temperature (rT) to discriminate live from dead cells. Cells were washed in CSB, incubated with human Fc receptor block (BioLegend) for 10 min at rT, and stained with a cell-surface antibody cocktail for 45 min at rT in a final volume of 100 µL (**Table S2**). Thereafter, intracellular staining was performed

with Fixation Buffer and Intracellular Staining Permeabilization Wash Buffer (BioLegend) and stained with an intracellular antibody cocktail for 30 min at rT. Cells were washed once in Perm buffer and twice in CSB, followed by incubation with 1 mL Maxpar Fix and Perm buffer (Fluidigm Sciences) containing 0.125 µM Cell-ID intercalator-Ir (Fluidigm) overnight at 4°C to discriminate singlets from doublets. The next day, cells were washed three times in CSB, and one time in de-ionized water immediately prior to data acquisition. Cells were acquired on a Helios mass cytometer (Fluidigm) at an event rate of <500 events/sec in de-ionized water containing 10x diluted EQ Four Element Calibration Beads (Fluidigm). Data were normalized with the normalization passport EQ-P13H2302_ver2 for each experiment.
Normalized FCS files were analyzed in FlowJo (version 10.6.1, Tree Star Inc). Data were checked for quality of staining and gated for live, single, $CD45^+$ cells using 191/193Ir DNA intercalator, CD45, event length, center, width, residual, 103Rh DNA intercalator, and 140Ce bead channels (gating strategy shown in **Figure S1**). Next, we specifically exported the $CD7^+CD3^-$ gate for each sample as FCS file for downstream analysis (**Figure S1**). $CD7^+CD3^-$ cells were hyberbolic ArcSinh transformed with a cofactor of 5, sample-tagged, and subjected to dimensionality reduction analysis in the Cytosplore software[48].

Sorting of ILCs from colorectal cancers for immunophenotyping and cell culturing
$CD7^+CD3^-CD127^{+/-}$ ILCs were sorted from MMR-deficient CRC tissues of six patients by FACS for immunophenotyping and cell culture (gating strategy shown in **Figure S2**). Cells were thawed, rest at 37°C in IMDM+L-glutamine (Lonza)/10% nHS for 1h, and washed in FACS buffer (PBS/1% FCS). Thereafter, cells were incubated with human Fc receptor block (BioLegend) and stained with the following cell surface antibodies: 1:20 anti-CD7-V450 [clone M-T701, BD Biosciences], 1:25 anti-CD3-Am Cyan [clone SK7, BD Biosciences] or 1:50 anti-CD3-PE [clone SK7, BD Biosciences], 1:20 anti-CD127-FITC [clone A019D5, Sony] or 1:150 anti-CD127-PE-Cy7 [clone A01905, BioLegend], 1:20 anti-CD45RO-PerCP-Cy5.5 [clone UCHL1, Sony], 1:20 anti-CD45RA-PE/Dazzle [clone HI100, Sony] or 1:30 anti-CD45RA-FITC [clone L48, BD Biosciences], and 1:150 anti-CD56-APC-R700 [clone NCAM16.2, BD Biosciences] for 45 min at 4°C together with different additional antibodies for immunophenotyping (including 1:200 anti-CD94-BV605 [clone HP-3D9, BD Biosciences], 1:20 anti-NKp44-PE [clone 253415, R&D Systems], 1:60 anti-CD39-APC [clone A1, BioLegend], 1:30 anti-NKG2A-APC [clone z199, Beckman Coulter], 1:150 anti-DNAM-1-BV510 [clone DX11, BD Biosciences], 1:10 anti-KIR3DL2-PE [clone #539304, R&D Systems], 1:10 anti-KIR2DL4-PE [clone #181703, R&D Systems], 1:50 anti-KIR2DL1/DS1-PE [clone EB6, Beckman Coulter], 1:40 anti-KIR2DL3-PE [clone GL183, Beckman Coulter], 1:20 anti-KIR3DL1/DS1-PE [clone Z27, Beckman Coulter], and 1:40 anti-KIR2DS4-PE [clone FES172, Beckman Coulter]. To discriminate live from dead cells, a live/dead fixable near-infrared viability dye (1:1000, Life Technologies) was included in each staining. Cells were washed three times in FACS buffer before sorting the cells on a FACS Aria III 4L (BD Biosciences). CompBeads (BD Biosciences) and ArC reactive beads (Life Technologies) were used for compensation controls. The ILCs were sorted in IMDM+L-glutamine medium containing feeder cells ($1x10^6$/mL), PHA (1 µg/mL; Thermo Fisher Scientific), gentamicin (50 µg/mL), and fungizone (0.5 µg/mL), and different cytokine mixes with: IL-2 (100 IU/mL and 500 IU/mL; Novartis), IL-15 (10 ng/mL; R&D Systems), IL-7 (10 ng/mL; Peprotech), IL-21 (10 ng/mL; Gibco), TNF-α (10 ng/mL; Peprotech), SCF (25 ng/mL; Miltenyi). The cytokine mixes tested included i) SCF (25 ng/mL), IL-2 (10 CU/mL), IL-7 (25 ng/mL) with feeder cells and PHA (1 µg/mL), ii) OP9-DL1 cells with SCF (25 ng/mL), IL-2 (10 CU/mL), IL-7 (25 ng/mL), iii) IL-2 (10 CU/mL) and IL-15 (10 ng/mL) with feeder cells and PHA (1 µg/mL), iv) TCGF (10%), IL-7 (10 ng/mL), IL-15 (10 ng/mL), IL-21 (10 ng/mL), TNF-α (10 ng/mL) with feeder cells/PHA (1 µg/mL) and EBV, and v) TCGF (10%), IL-7 (10 ng/mL), IL-15 (10 ng/mL), IL-21 (10 ng/mL), TNF-α (10 ng/mL) with feeder cells and PHA (1 µg/mL). During and after 3-4 weeks expansion, the purity and phenotype of the ILCs were assessed by flow cytometry.

Sorting of ILCs from colorectal cancers for single-cell RNA-sequencing
$CD7^+CD3^-CD127^{+/-}$ ILCs were sorted from MMR-deficient CRC tissues of five patients by FACS and processed for single-cell RNA-sequencing (scRNA-seq). Hashtag oligo (HTOs) antibodies were included

for sample ID, and antibody-derived tags (ADTs) for CD45RA and CD45RO protein expression using CITE-seq[49] (**Figure S3**), as described previously.[50] In short, cell suspensions were thawed, rest at 37°C in IMDM (Lonza)/20% FCS for 1h, and washed in FACS buffer (PBS (Fresenius Kabi)/1% FCS). Cells were subsequently incubated with human Fc receptor block (BioLegend) for 10 min at 4°C. Thereafter, cells were stained with the following cell surface antibodies: 1:160 anti-CD45-PerCP-Cy5.5 [clone 2D1, eBioscience], 1:50 anti-CD3-PE [clone SK7, BD Biosciences], 1:200 anti-CD7-APC [clone 124-1D1, eBioscience], 1:60 anti-EPCAM-FITC [clone HEA-125, Miltenyi], and 1:80 anti-TCRγδ-BV421 [clone 11F2, BD Biosciences]. In parallel, the following ADTs for CD45RA and CD45RO were added in the antibody mix: 1 µg of TotalSeq-C anti-CD45RA (clone HI100, BioLegend) and 1 µg of anti-CD45RO (clone UCHL1, BioLegend), together with the following HTOs: 0.5 µg of a unique TotalSeq-C CD298/β2M hashtag antibody (clone LNH-94/2M2, BioLegend) for each sample (N=5) for 30 min at 4°C. To discriminate live from dead cells, a live/dead fixable near-infrared viability dye (1:1000, Life Technologies) was included in each staining. Cells were washed three times in FACS buffer before sorting the cells. CompBeads (BD Biosciences) and ArC reactive beads (Life Technologies) were used for compensation controls. Single, live $EPCAM^{-}CD45^{+}CD7^{+}CD3^{-}$ cells were sorted on a FACS Aria III 4L (BD Biosciences). After sorting, the samples were pooled in FACS buffer, washed, and resuspended in PBS with 0.04% BSA at a concentration of 1,000 cells/µL for downstream application.

Single-cell RNA-sequencing data analysis

Libraries were prepared using the Chromium Single Cell 5' Reagent Kit v1 chemistry (10X Genomics), following the manufacturer's instructions, and sequenced on a HiSeq X Ten using paired-end 2x150 bp sequencing (Illumina) as described previously.[50] Briefly, reads were aligned to the human reference genome (GRCh38) and quantified using Cell Ranger (version 3.1.0). Seurat (version 4.0.4)[51] was used for downstream analysis. Cells with less than 200 detected genes and genes expressed in less than six cells were excluded, resulting in a dataset of 5748 cells. These were demultiplexed based on HTO enrichment using the MULTIseqDemux algorithm[52], resulting in 4755 cells excluding doublet and negative HTOs. Next, a patient-specific analysis approach was performed were cells with a mitochondrial gene content greater than 10% and cells with outlying numbers of expressed genes (>3000) were filtered out for each patient. Transcriptomes from 1293 cells (HTO1), 228 cells (HTO6), 502 cells (HTO7), 1059 cells (HTO8), and 1188 cells (HTO9) were used for further analysis (**Figure S3**). Data normalization was performed using the 'LogNormalize' function with scale factor 10,000. The 'FindVariableFeatures' function was used to identify 2,000 variable features in the data. Data were scaled and heterogeneity associated with mitochondrial contamination was regressed out. Next, PCA was run on the scaled data and the optimal number of dimensions was determined for each patient individually. Clustering was performed with the 'FindNeighbors' and 'FindClusters' functions, where the optimal resolution parameter was set for each patient individually. Non-linear dimensional reduction with t-SNE[53] and uniform manifold approximation (UMAP)[54] were used to visualize the cells. Differentially expressed genes were identified with the 'FindAllMarkers' function with min.pct and logfc.threshold at 0.25.

Validation in a publicly available single-cell RNA-sequencing CRC dataset

We validated our findings in the publicly available scRNA-seq CRC dataset of Pelka *et al.*[28] consisting of MMR-deficient CRC (N=35), MMR-proficient CRC (N=29), and adjacent healthy tissue (N=36). Briefly, cells of main partition T/NK/ILC were extracted for all samples. In Seurat (version 4.0.3), $CD7^{+}CD3\delta^{-}$ cells were selected and re-clustered with resolution parameter 0.4. Non-linear dimensional reduction with t-SNE was used to visualize the clustered cells. Differentially expressed genes were identified with the 'FindAllMarkers' function with min.pct and logfc.threshold at 0.25.

ACKNOWLEDGEMENTS

We thank K.C.M.J. Peeters, M.G. Kallenberg-Lantrua, D. Berends-van der Meer, and F.A. Holman for their help in collecting and providing samples from patients with colorectal cancer; the Flow cytometry

Core Facility of the Leiden University Medical Center for their help with cell sorting; the Leiden Genome Technology Center for their help with single-cell RNA-sequencing; A. Mahfouz for his help with the scRNA-sequencing analysis.

AUTHOR CONTRIBUTIONS

N.L. de Vries conceived the study and performed experiments. N.L. de Vries, L. Zheng, J. Roelands, and D. Ruano performed the computational analyses presented in this paper. N.L. de Vries, L. Zheng, J. Roelands, D. Ruano, N.F. de Miranda, and F. Koning analyzed and interpreted the data. M. van der Ploeg, M.E. Ijsselsteijn, and R. van der Breggen assisted with experiments. J. Krop designed the mass cytometry antibody panel under supervision of M. Eikmans. F. Koning and N.F. de Miranda supervised the study. The manuscript was written by N.L. de Vries, F. Koning, and N.F. de Miranda in collaboration with all co-authors.

COMPETING INTERESTS

The authors declare no competing interests exist.

REFERENCES

1 Fridman, W. H., Zitvogel, L., Sautes-Fridman, C. & Kroemer, G. The immune contexture in cancer prognosis and treatment. *Nature reviews. Clinical oncology* 14, 717-734, doi:10.1038/nrclinonc.2017.101 (2017).

2 Dolcetti, R. *et al.* High prevalence of activated intraepithelial cytotoxic T lymphocytes and increased neoplastic cell apoptosis in colorectal carcinomas with microsatellite instability. *Am J Pathol* 154, 1805-1813, doi:10.1016/s0002-9440(10)65436-3 (1999).

3 Tumeh, P. C. *et al.* PD-1 blockade induces responses by inhibiting adaptive immune resistance. *Nature* 515, 568-571, doi:10.1038/nature13954 (2014).

4 Taube, J. M. *et al.* Association of PD-1, PD-1 ligands, and other features of the tumor immune microenvironment with response to anti-PD-1 therapy. *Clin Cancer Res* 20, 5064-5074, doi:10.1158/1078-0432.Ccr-13-3271 (2014).

5 Ionov, Y., Peinado, M. A., Malkhosyan, S., Shibata, D. & Perucho, M. Ubiquitous somatic mutations in simple repeated sequences reveal a new mechanism for colonic carcinogenesis. *Nature* 363, 558-561, doi:10.1038/363558a0 (1993).

6 Germano, G. *et al.* Inactivation of DNA repair triggers neoantigen generation and impairs tumour growth. *Nature* 552, 116-120, doi:10.1038/nature24673 (2017).

7 Le, D. T. *et al.* Mismatch repair deficiency predicts response of solid tumors to PD-1 blockade. *Science* 357, 409-413, doi:10.1126/science.aan6733 (2017).

8 Overman, M. J. *et al.* Nivolumab in patients with metastatic DNA mismatch repair-deficient or microsatellite instability-high colorectal cancer (CheckMate 142): an open-label, multicentre, phase 2 study. *The Lancet. Oncology* 18, 1182-1191, doi:10.1016/s1470-2045(17)30422-9 (2017).

9 Overman, M. J. *et al.* Durable Clinical Benefit With Nivolumab Plus Ipilimumab in DNA Mismatch Repair-Deficient/Microsatellite Instability-High Metastatic Colorectal Cancer. *Journal of clinical oncology : official journal of the American Society of Clinical Oncology* 36, 773-779, doi:10.1200/jco.2017.76.9901 (2018).

10 Chalabi, M. *et al.* Neoadjuvant immunotherapy leads to pathological responses in MMR-proficient and MMR-deficient early-stage colon cancers. *Nat Med* 26, 566-576, doi:10.1038/s41591-020-0805-8 (2020).

11 Bicknell, D. C., Kaklamanis, L., Hampson, R., Bodmer, W. F. & Karran, P. Selection for beta 2-microglobulin mutation in mismatch repair-defective colorectal carcinomas. *Current biology : CB* 6, 1695-1697, doi:10.1016/s0960-9822(02)70795-1 (1996).

12 Dierssen, J. W. *et al.* HNPCC versus sporadic microsatellite-unstable colon cancers follow different routes toward loss of HLA class I expression. *BMC Cancer* 7, 33, doi:10.1186/1471-2407-7-33 (2007).

13 Kloor, M. *et al.* Immunoselective pressure and human leukocyte antigen class I antigen machinery defects in microsatellite unstable colorectal cancers. *Cancer Res* 65, 6418-6424, doi:10.1158/0008-5472.can-05-0044 (2005).

14 Ijsselsteijn, M. E. *et al.* Revisiting immune escape in colorectal cancer in the era of immunotherapy. *Br J Cancer* 120, 815-818, doi:10.1038/s41416-019-0421-x (2019).

15 Middha, S. *et al.* Majority of B2M-Mutant and -Deficient Colorectal Carcinomas Achieve Clinical Benefit From Immune Checkpoint Inhibitor Therapy and Are Microsatellite Instability-High. *JCO precision oncology* 3, doi:10.1200/po.18.00321 (2019).

16 de Vries, N. L. *et al.* High-dimensional cytometric analysis of colorectal cancer reveals novel mediators of antitumour immunity. *Gut* 69, 691-703, doi:10.1136/gutjnl-2019-318672 (2020).

17 Vivier, E. *et al.* Innate Lymphoid Cells: 10 Years On. *Cell* 174, 1054-1066, doi:10.1016/j.cell.2018.07.017 (2018).

18 Glatzer, T. *et al.* RORγt$^+$ innate lymphoid cells acquire a proinflammatory program upon engagement of the activating receptor NKp44. *Immunity* 38, 1223-1235, doi:10.1016/j.immuni.2013.05.013 (2013).

19 Spits, H. *et al.* Innate lymphoid cells--a proposal for uniform nomenclature. *Nat Rev Immunol* 13, 145-149, doi:10.1038/nri3365 (2013).

20 Fuchs, A. *et al.* Intraepithelial type 1 innate lymphoid cells are a unique subset of IL-12- and IL-15-responsive IFN-gamma-producing cells. *Immunity* 38, 769-781, doi:10.1016/j.immuni.2013.02.010 (2013).

21 Hazenberg, M. D. & Spits, H. Human innate lymphoid cells. *Blood* 124, 700-709, doi:10.1182/blood-2013-11-427781 (2014).

22 Cella, M. *et al.* Subsets of ILC3-ILC1-like cells generate a diversity spectrum of innate lymphoid cells in human mucosal tissues. *Nat Immunol* 20, 980-991, doi:10.1038/s41590-019-0425-y (2019).

23 Bernink, J. H. *et al.* Interleukin-12 and -23 Control Plasticity of CD127(+) Group 1 and Group 3 Innate Lymphoid Cells in the Intestinal Lamina Propria. *Immunity* 43, 146-160, doi:10.1016/j.

immuni.2015.06.019 (2015).

24 Crinier, A. *et al.* High-Dimensional Single-Cell Analysis Identifies Organ-Specific Signatures and Conserved NK Cell Subsets in Humans and Mice. *Immunity* 49, 971-986.e975, doi:10.1016/j.immuni.2018.09.009 (2018).

25 Krabbendam, L. *et al.* CD127+ CD94+ innate lymphoid cells expressing granulysin and perforin are expanded in patients with Crohn's disease. *Nat Commun* 12, 5841, doi:10.1038/s41467-021-26187-x (2021).

26 Lee, N. *et al.* HLA-E is a major ligand for the natural killer inhibitory receptor CD94/NKG2A. *Proc Natl Acad Sci U S A* 95, 5199-5204, doi:10.1073/pnas.95.9.5199 (1998).

27 Rajagopalan, S. & Long, E. O. KIR2DL4 (CD158d): An activation receptor for HLA-G. *Front Immunol* 3, 258, doi:10.3389/fimmu.2012.00258 (2012).

28 Pelka, K. *et al.* Spatially organized multicellular immune hubs in human colorectal cancer. *Cell* 184, 4734-4752.e4720, doi:10.1016/j.cell.2021.08.003 (2021).

29 Qi, J. *et al.* Single-cell transcriptomic landscape reveals tumor specific innate lymphoid cells associated with colorectal cancer progression. *Cell Rep Med* 2, 100353, doi:10.1016/j.xcrm.2021.100353 (2021).

30 Mazzurana, L. *et al.* Tissue-specific transcriptional imprinting and heterogeneity in human innate lymphoid cells revealed by full-length single-cell RNA-sequencing. *Cell Res* 31, 554-568, doi:10.1038/s41422-020-00445-x (2021).

31 Simoni, Y. *et al.* Human Innate Lymphoid Cell Subsets Possess Tissue-Type Based Heterogeneity in Phenotype and Frequency. *Immunity* 46, 148-161, doi:10.1016/j.immuni.2016.11.005 (2017).

32 Sheridan, B. S. & Lefrançois, L. Intraepithelial lymphocytes: to serve and protect. *Curr Gastroenterol Rep* 12, 513-521, doi:10.1007/s11894-010-0148-6 (2010).

33 Dadi, S. *et al.* Cancer Immunosurveillance by Tissue-Resident Innate Lymphoid Cells and Innate-like T Cells. *Cell* 164, 365-377, doi:10.1016/j.cell.2016.01.002 (2016).

34 Flommersfeld, S. *et al.* Fate mapping of single NK cells identifies a type 1 innate lymphoid-like lineage that bridges innate and adaptive recognition of viral infection. *Immunity* 54, 2288-2304.e2287, doi:10.1016/j.immuni.2021.08.002 (2021).

35 Roan, F. *et al.* CD4+ Group 1 Innate Lymphoid Cells (ILC) Form a Functionally Distinct ILC Subset That Is Increased in Systemic Sclerosis. *J Immunol* 196, 2051-2062, doi:10.4049/jimmunol.1501491 (2016).

36 Bekiaris, V. *et al.* Human CD4+CD3- innate-like T cells provide a source of TNF and lymphotoxin-αβ and are elevated in rheumatoid arthritis. *J Immunol* 191, 4611-4618, doi:10.4049/jimmunol.1301672 (2013).

37 Björklund Å, K. *et al.* The heterogeneity of human CD127(+) innate lymphoid cells revealed by single-cell RNA sequencing. *Nat Immunol* 17, 451-460, doi:10.1038/ni.3368 (2016).

38 Moral, J. A. *et al.* ILC2s amplify PD-1 blockade by activating tissue-specific cancer immunity. *Nature* 579, 130-135, doi:10.1038/s41586-020-2015-4 (2020).

39 Hsu, J. *et al.* Contribution of NK cells to immunotherapy mediated by PD-1/PD-L1 blockade. *J Clin Invest* 128, 4654-4668, doi:10.1172/jci99317 (2018).

40 Davis-Marcisak, E. F. *et al.* Transfer learning between preclinical models and human tumors identifies a conserved NK cell activation signature in anti-CTLA-4 responsive tumors. *Genome Med* 13, 129, doi:10.1186/s13073-021-00944-5 (2021).

41 Kamiya, T., Seow, S. V., Wong, D., Robinson, M. & Campana, D. Blocking expression of inhibitory receptor NKG2A overcomes tumor resistance to NK cells. *J Clin Invest* 129, 2094-2106, doi:10.1172/jci123955 (2019).

42 Carrega, P. *et al.* Characterisation of innate lymphoid cell subsets infiltrating colorectal carcinoma. *Gut* 69, 2261-2263, doi:10.1136/gutjnl-2020-320908 (2020).

43 Wang, S. *et al.* Transdifferentiation of tumor infiltrating innate lymphoid cells during progression of colorectal cancer. *Cell Res* 30, 610-622, doi:10.1038/s41422-020-0312-y (2020).

44 Ikeda, A. *et al.* Human NKp44(+) Group 3 Innate Lymphoid Cells Associate with Tumor-Associated Tertiary Lymphoid Structures in Colorectal Cancer. *Cancer Immunol Res* 8, 724-731, doi:10.1158/2326-6066.Cir-19-0775 (2020).

45 Bernink, J. H. *et al.* Human type 1 innate lymphoid cells accumulate in inflamed mucosal tissues. *Nat Immunol* 14, 221-229, doi:10.1038/ni.2534 (2013).

46 Gao, Y. *et al.* Tumor immunoevasion by the conversion of effector NK cells into type 1 innate lymphoid cells. *Nat Immunol* 18, 1004-1015, doi:10.1038/ni.3800 (2017).

47 Hall, G. *et al.* Immunohistochemistry for PMS2 and MSH6 alone can replace a four antibody panel for mismatch repair deficiency screening in colorectal adenocarcinoma. *Pathology* 42, 409-413, doi:10.3109/00313025.2010.493871 (2010).

48 Höllt, T. *et al.* Cytosplore: Interactive Immune Cell Phenotyping for Large Single-Cell Datasets. 35, 171-180, doi:https://doi.org/10.1111/cgf.12893 (2016).

49 Stoeckius, M. *et al.* Simultaneous epitope and transcriptome measurement in single cells. *Nat Methods* 14, 865-868, doi:10.1038/nmeth.4380

(2017).

50 de Vries, N. L. *et al.* γδ T cells are effectors of immune checkpoint blockade in mismatch repair-deficient colon cancers with antigen presentation defects. *bioRxiv*, 2021.2010.2014.464229, doi:10.1101/2021.10.14.464229 (2021).

51 Stuart, T. *et al.* Comprehensive Integration of Single-Cell Data. *Cell* 177, 1888-1902 e1821, doi:10.1016/j.cell.2019.05.031 (2019).

52 McGinnis, C. S. *et al.* MULTI-seq: sample multiplexing for single-cell RNA sequencing using lipid-tagged indices. *Nat Methods* 16, 619-626, doi:10.1038/s41592-019-0433-8 (2019).

53 van der Maaten, L. J. P. & Hinton, G. E. Visualizing high-dimensional data using t-SNE. *J. Mach. Learn. Res.* 9, 2579-2605 (2008).

54 McInnes, L., Healy, J. & Melville, J. J. a. p. a. Umap: Uniform manifold approximation and projection for dimension reduction. (2018).

SUPPLEMENTAL FIGURES

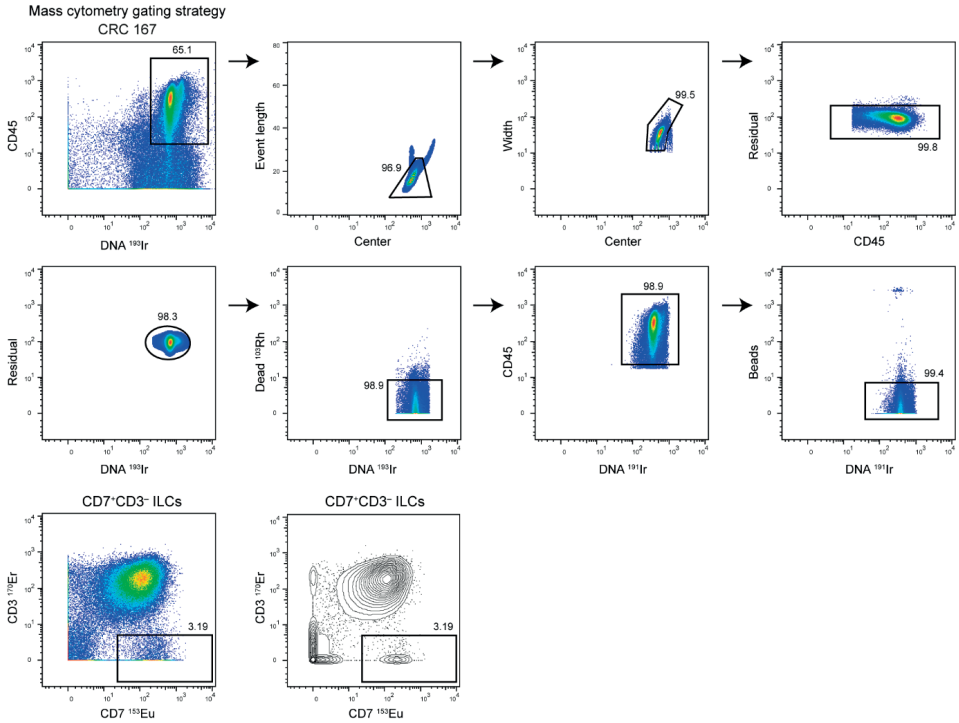

Figure S1. Mass cytometry gating strategy for the ILC population from MMR-deficient colorectal cancers. Mass cytometry gating strategy for single, live CD45$^+$CD7$^+$CD3$^-$ ILCs of a representative MMR-deficient colorectal cancer sample showing sequential gates with percentages.

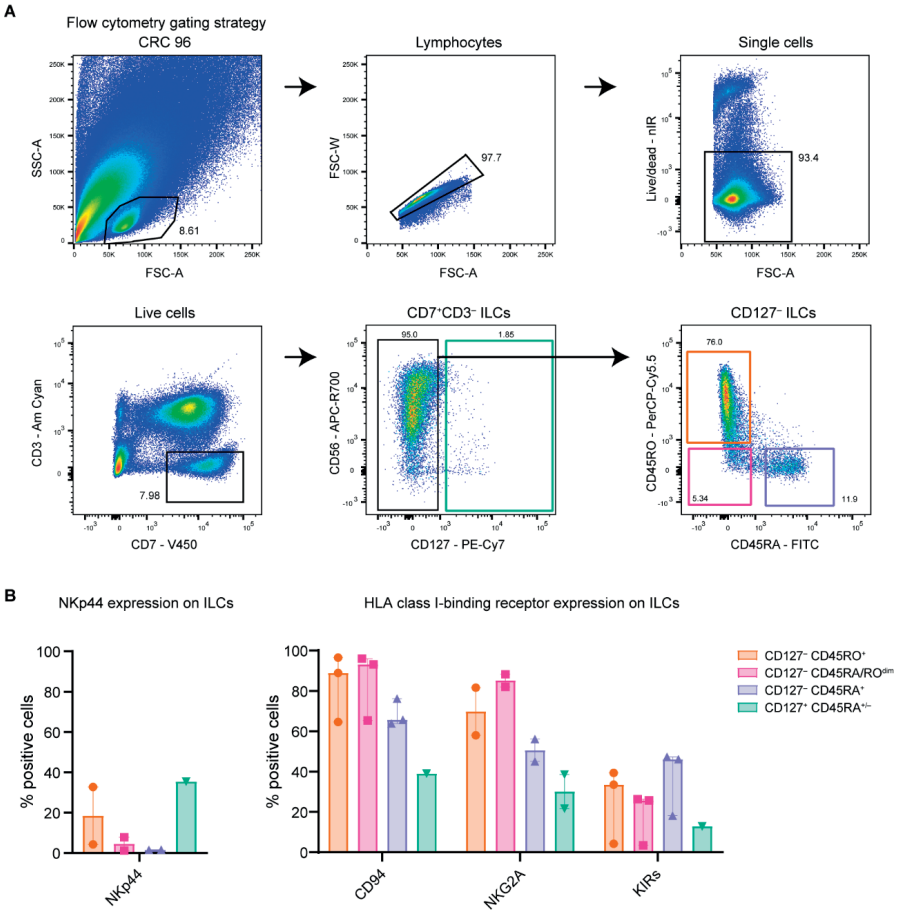

Figure S2. Flow cytometry gating strategy and frequencies of NKp44 and HLA class I-binding receptors on ILC subsets from MMR-deficient colorectal cancers.

A. Flow cytometry gating strategy for CD127$^-$CD45RO$^+$ ILC1-like (orange), CD127$^-$CD45RA/RO^{dim} ILC1-like (pink), CD127$^-$CD45RA$^+$ NK-like (purple), and CD127$^+$CD45RA$^{+/-}$ ILC2 (green) cells showing sequential gates with percentages. **B**. Frequencies of NKp44 and HLA class I-binding receptors among CD127$^-$CD45RO$^+$ ILC1-like (orange), CD127$^-$CD45RA/RO^{dim} ILC1-like (pink), CD127$^-$CD45RA$^+$ NK-like (purple), and CD127$^+$CD45RA$^{+/-}$ ILC2 (green) cells as percentage of total ILCs from MMR-deficient CRCs *ex vivo* (N=2-3) by flow cytometry. Marker frequencies for ILC2s (green) were only included when >100 cells were present. Bars indicate the median with IQR. Data from five independent experiments.

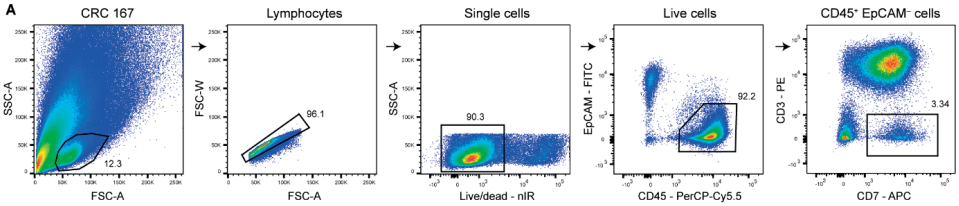

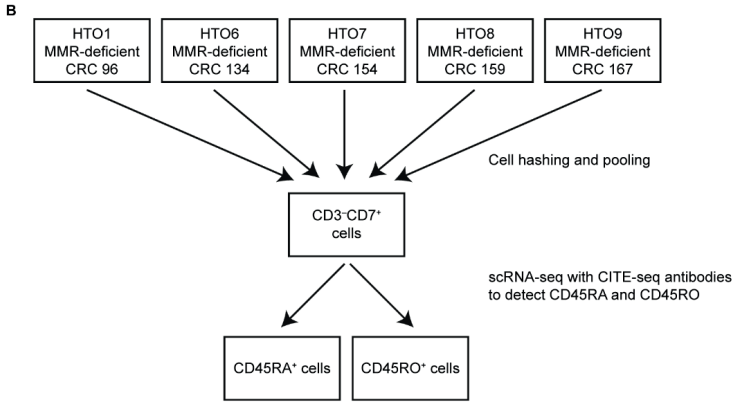

C

Patient ID	HTO1 CRC 96	HTO6 CRC 134	HTO7 CRC 154	HTO8 CRC 159	HTO9 CRC 167
Cell number at FACS sorting:	6662 cells	3307 cells	3226 cells	6140 cells	6656 cells
Cell number at scRNA-seq analysis:	1293 cells	228 cells	502 cells	1059 cells	1188 cells
Fraction in:	19.4%	6.9%	15.6%	17.2%	17.8%

Figure S3. Gating strategy and experimental design for single-cell RNA-sequencing of the ILC population from MMR-deficient colorectal cancers.

A. FACS gating strategy for single, live CD45$^+$EpCAM$^-$CD7$^+$CD3$^-$ ILCs of a representative MMR-deficient colorectal cancer sample showing sequential gates with percentages. **B**. Experimental design of the single-cell RNA-sequencing study with HTO- and CITE-sequencing antibodies performed on CD7$^+$CD3$^-$ cells isolated from MMR-deficient CRCs (N=5). **C**. Table showing the number of CD7$^+$CD3$^-$ cells isolated from MMR-deficient CRCs at the time of sorting *versus* the number of cells in the single-cell RNA-sequencing analysis, and the fraction thereof.

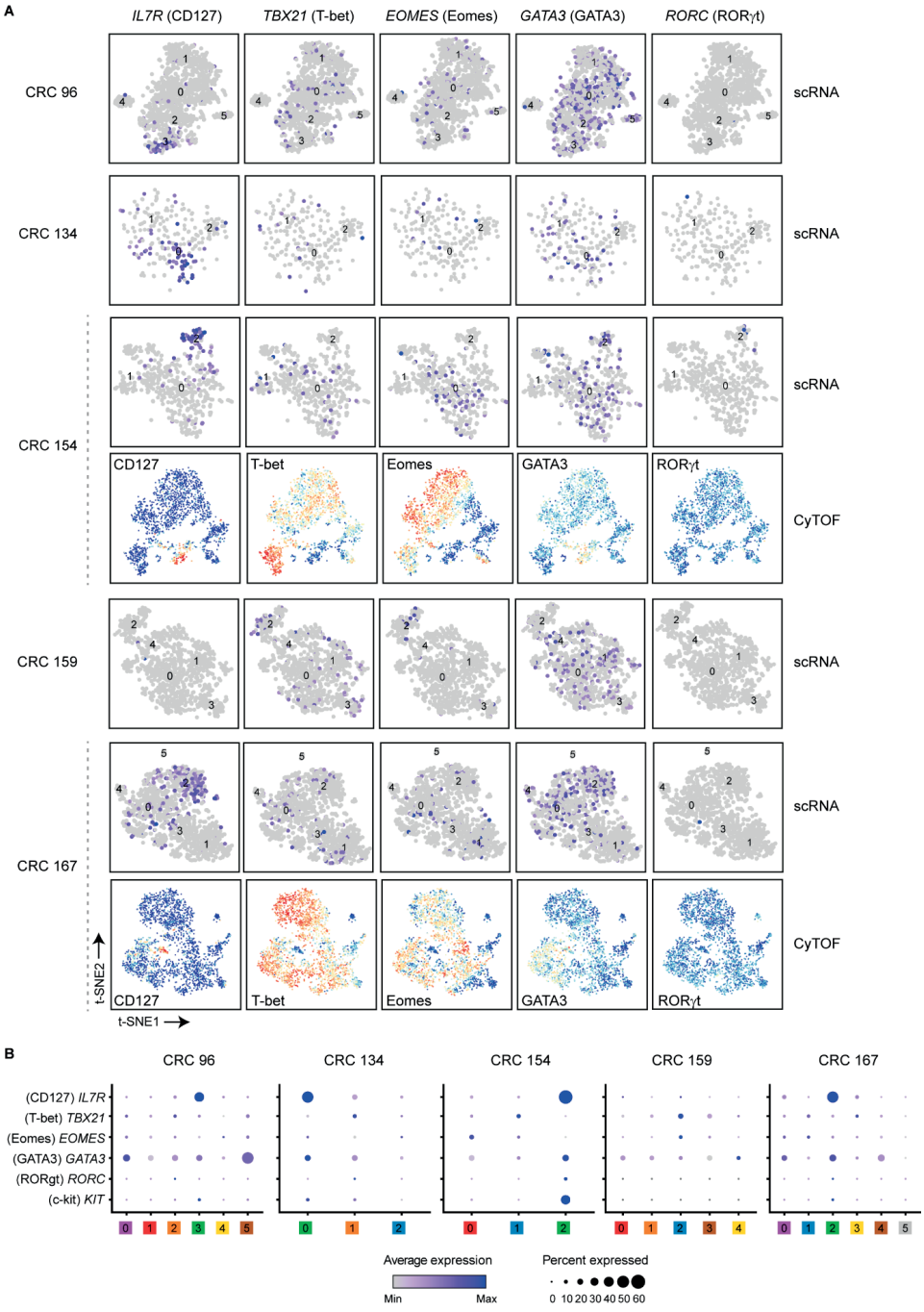

Figure S4. Transcription factor analysis of ILCs from MMR-deficient colorectal cancers by single-cell RNA-sequencing and mass cytometry.

A. t-SNE embedding showing the relative expression of indicated markers on CD7^{+}CD3^{-} ILCs isolated from MMR-deficient CRCs (N=5) analyzed by single-cell RNA-sequencing (scRNA; gene expression) per patient, and as compared

to mass cytometry (CyTOF; protein expression) for two paired samples. Colors represent relative expression of indicated genes (scRNA) and proteins (CyTOF). Each dot represents a single cell. **B**. Dot plots showing the relative expression of indicated genes in the clusters identified in **Figure 2**. Color intensity indicates average expression and size of the dot indicates the percentage of cells expressing the gene.

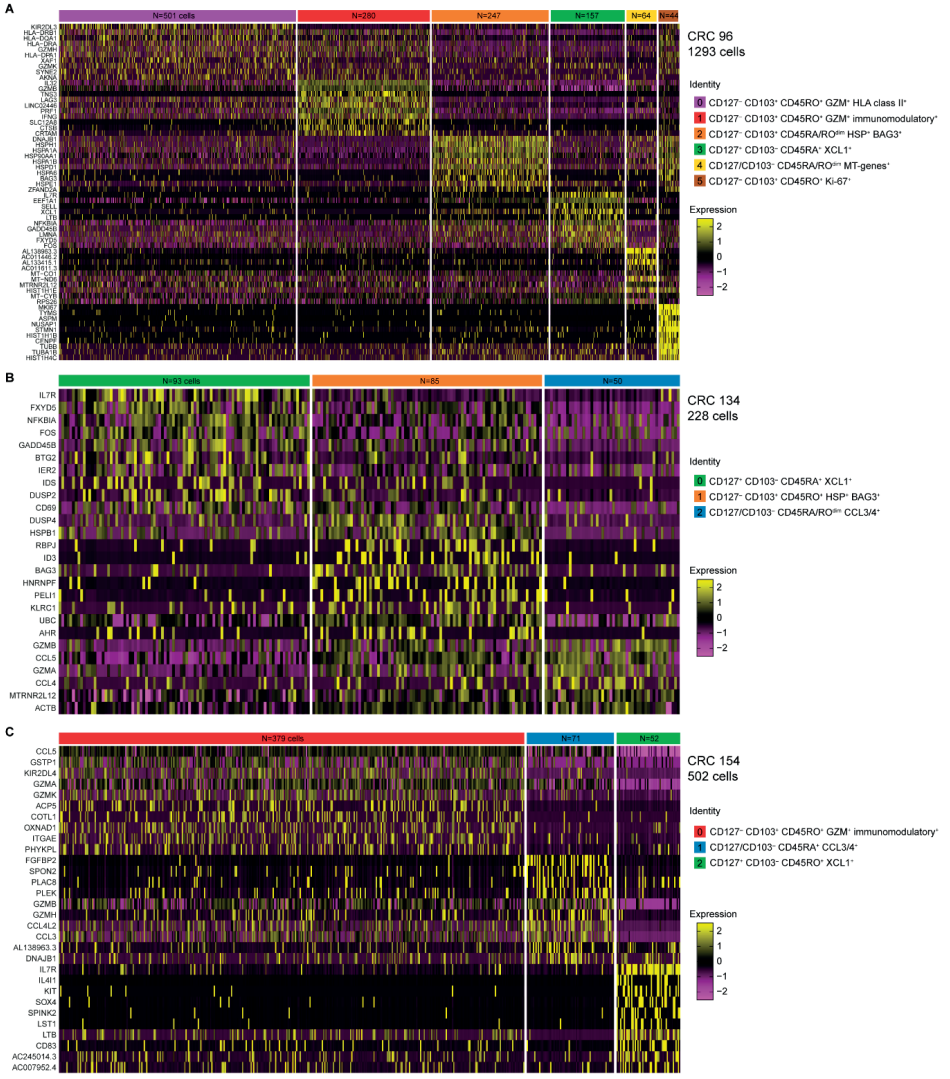

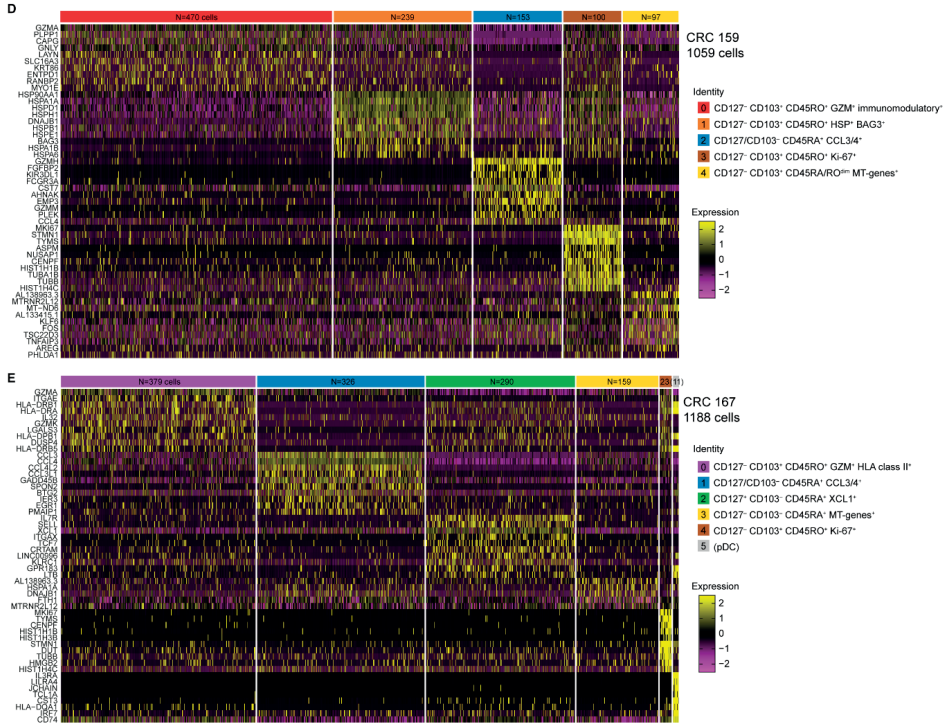

Figure S5. Distinct ILC clusters in MMR-deficient colorectal cancers by single-cell RNA-sequencing.
A. Heatmap showing the normalized single-cell gene expression value (z-score, purple-to-yellow scale) for the top 10 differentially expressed genes in each identified CD7⁺CD3⁻ ILC cluster for MMR-deficient CRC 96 (N=1293 cells). Color bar at the top represents functionally distinct categories of ILC subsets. **B**. As (**A**), but for MMR-deficient CRC 134 (N=228 cells). **C**. As (**A**), but for MMR-deficient CRC 154 (N=502 cells). **D**. As (**A**), but for MMR-deficient CRC 159 (N=1059 cells). **E**. As (**A**), but for MMR-deficient CRC 167 (N=1188 cells).

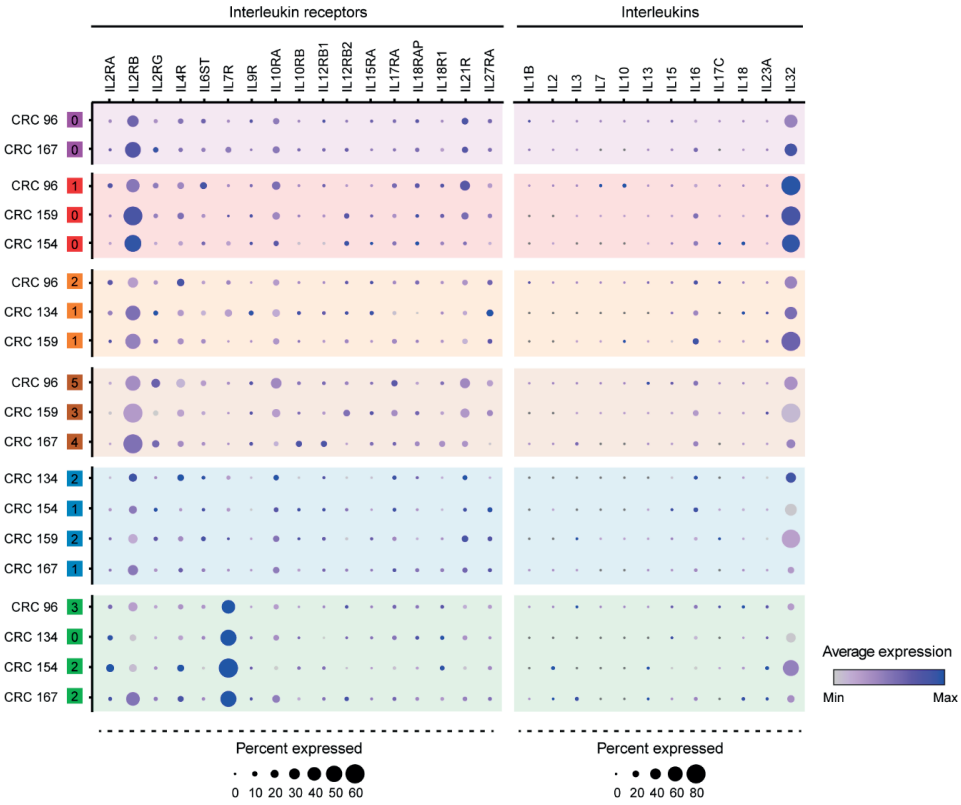

Figure S6. Transcriptional profiles of interleukin receptors and interleukins by ILCs from MMR-deficient colorectal cancers.

Dot plots showing the relative expression of indicated genes in the clusters identified in (**Figure 3A**). Color intensity indicates average expression and size of the dot indicates the percentage of cells expressing the gene. Background colors indicate functionally distinct categories of ILC subsets as in (**Figure 3A**). Interleukin receptor and interleukin transcripts with a median percentage of at least 1% of positive ILCs (N=4270) were included.

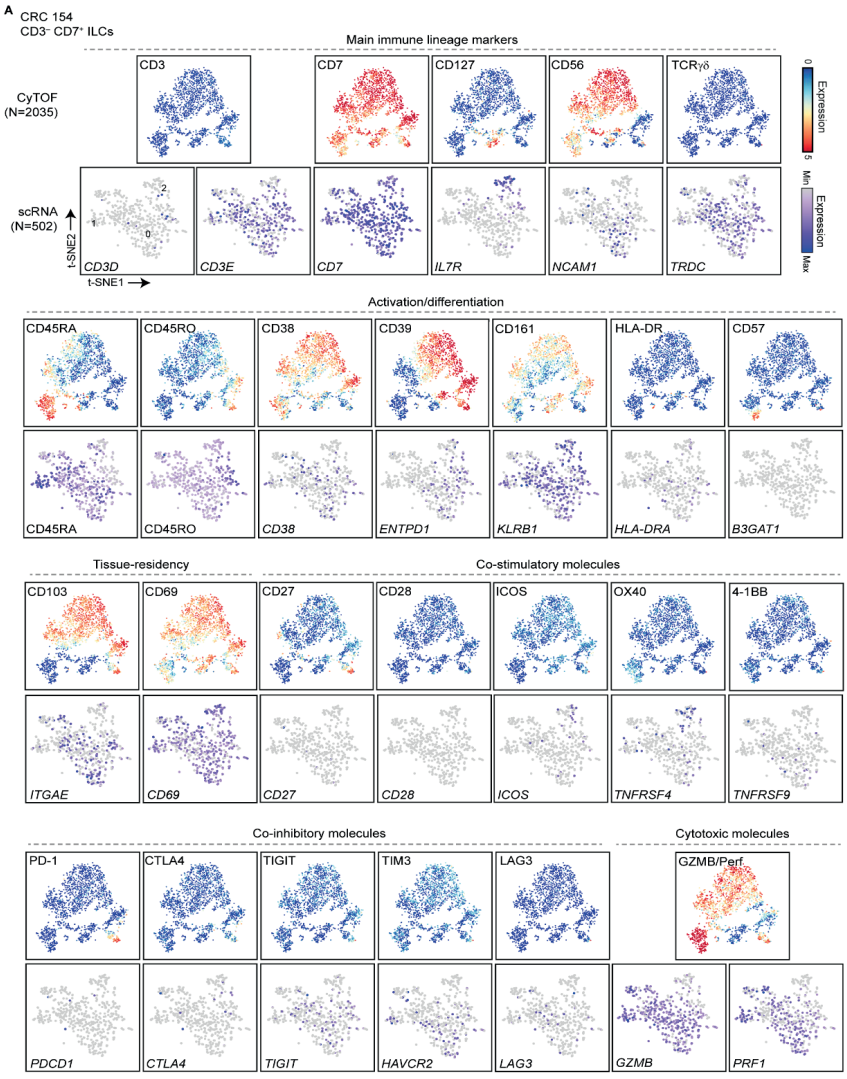
A
CRC 154
CD3⁻ CD7⁺ ILCs
Main immune lineage markers
CyTOF
(N=2035)
CD3
CD7
CD127
CD56
TCRγδ
Expression
scRNA
(N=502)
t-SNE2
t-SNE1
CD3D
CD3E
CD7
IL7R
NCAM1
TRDC
Min
Max
Activation/differentiation
CD45RA
CD45RO
CD38
CD39
CD161
HLA-DR
CD57
CD45RA
CD45RO
CD38
ENTPD1
KLRB1
HLA-DRA
B3GAT1
Tissue-residency
Co-stimulatory molecules
CD103
CD69
CD27
CD28
ICOS
OX40
4-1BB
ITGAE
CD69
CD27
CD28
ICOS
TNFRSF4
TNFRSF9
Co-inhibitory molecules
Cytotoxic molecules
PD-1
CTLA4
TIGIT
TIM3
LAG3
GZMB/Perf
PDCD1
CTLA4
TIGIT
HAVCR2
LAG3
GZMB
PRF1

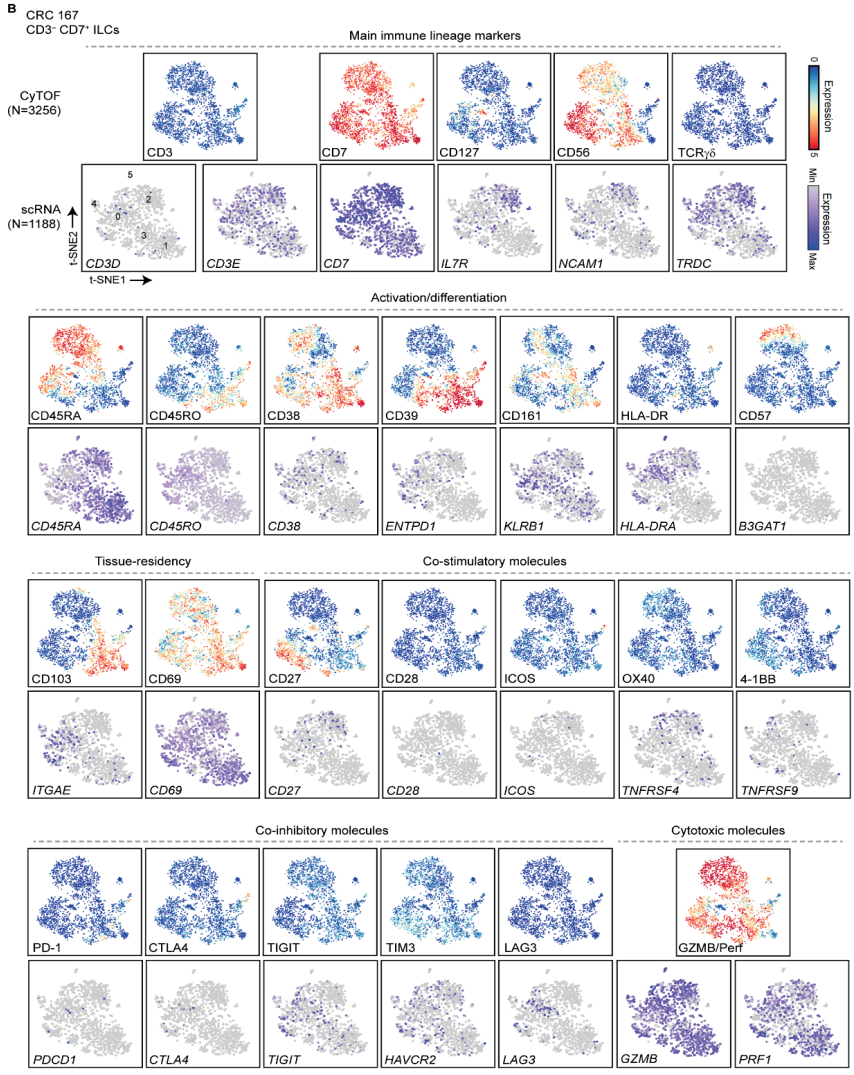

Figure S7. Mass cytometric *versus* transcriptional profiles of immune cell markers on ILCs in MMR-deficient colorectal cancers.

A. t-SNE embedding showing the relative expression of indicated immune cell markers on CD7⁺CD3⁻ ILCs analyzed by mass cytometry (CyTOF, N=2035) as compared to CD7⁺CD3⁻ ILCs analyzed by single-cell RNA-sequencing (scRNA, N=502) isolated from MMR-deficient CRC 154. Colors represent relative expression of indicated genes (scRNA) and proteins (CyTOF). Each dot represents a single cell. **B**. As (**A**), but for CD7⁺CD3⁻ ILCs analyzed by mass cytometry (CyTOF, N=3256) as compared to CD7⁺CD3⁻ ILCs analyzed by single-cell RNA-sequencing (scRNA, N=1188) isolated from MMR-deficient CRC 167.

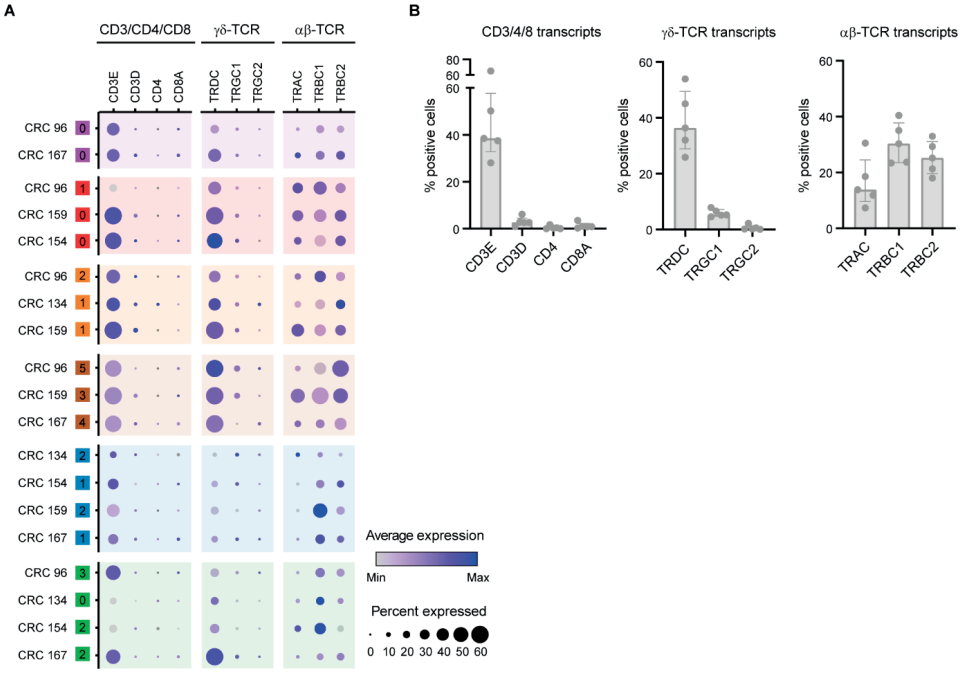

Figure S8. Transcriptional profiles of CD3 and T cell receptors by ILCs from MMR-deficient colorectal cancers. **A**. Dot plots showing the relative expression of indicated genes in the clusters identified in (**Figure 3A**). Color intensity indicates average expression and size of the dot indicates the percentage of cells expressing the gene. Background colors indicate functionally distinct categories of ILC subsets as in (**Figure 3A**). **B**. Frequencies of CD3, γδ-TCR, and αβ-TCR gene expression among all ILCs (N=4270) as percentage of positive cells from MMR-deficient CRCs (N=5). Bars indicate the median with IQR.

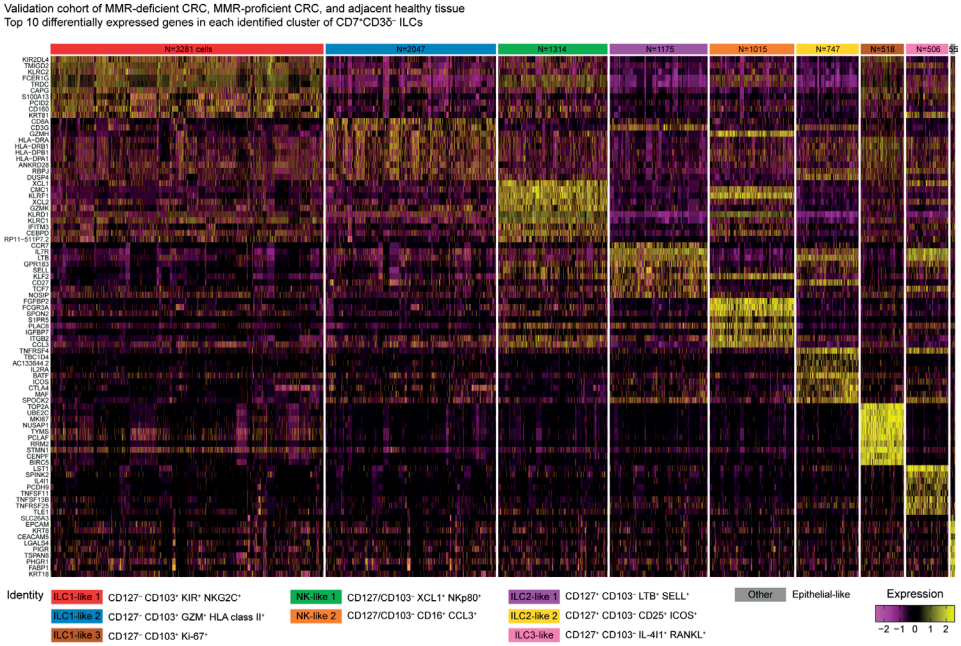

Figure S9. Distinct ILC clusters in MMR-deficient and -proficient colorectal cancers and adjacent healthy tissues by single-cell RNA-sequencing.

Heatmap showing the normalized single-cell gene expression value (z-score, purple-to-yellow scale) for the top 10 differentially expressed genes in each identified cluster from **Figure 4** of CD7^{+}CD3δ^{-} ILCs (N=10660) from MMR-deficient CRCs (N=35), MMR-proficient CRCs (N=29), and adjacent healthy tissues (N=36) obtained from the single-cell RNA-sequencing dataset of Pelka *et al.*[28].

SUPPLEMENTAL TABLES

The supplementary tables are available in the appendix to this thesis at the repository of Leiden University (https://hdl.handle.net/1887/3439882) and can be requested from the author.

Table S1: Characteristics of clinical samples from patients with MMR-deficient colorectal cancer included in the study.
Table S2: Antibodies used for mass cytometry experiments.